INL/JOU-21-61654-Revision-0

Spread Spectrum Symbol Detection with Blind Interference Suppression in FBMC-SS

July 2021

David B. Haab, Hussein Moradi, Behrouz Farhang-Boroujeny

Changing the World's Energy Future

Idaho National Laboratory

INL is a U.S. Department of Energy National Laboratory operated by Battelle Energy Alliance, LLC

INL/JOU-21-61654-Revision-0

Spread Spectrum Symbol Detection with Blind Interference Suppression in FBMC-SS

David B. Haab, Hussein Moradi, Behrouz Farhang-Boroujeny

July 2021

Idaho National Laboratory
Idaho Falls, Idaho 83415

http://www.inl.gov

Prepared for the
U.S. Department of Energy
Under DOE Idaho Operations Office
Contract DE-AC07-05ID14517

Received 11 May 2021; revised 11 June 2021; accepted 14 June 2021. Date of current version 19 July 2021.

Digital Object Identifier 10.1109/OJCOMS.2021.3090356

Spread Spectrum Symbol Detection With Blind Interference Suppression in FBMC-SS

DAVID B. HAAB [1], HUSSEIN MORADI [2] (Member, IEEE), AND BEHROUZ FARHANG-BOROUJENY [1] (Life Senior Member, IEEE)

[1] Electrical and Computer Engineering Department, University of Utah, Salt Lake City, UT 84112, USA

[2] Spectrum Innovation Department, Idaho National Laboratory, Idaho Falls, ID 83415, USA

CORRESPONDING AUTHOR: D. B. HAAB (e-mail: dvhaab@gmail.com)

This work was supported in part by the Department Defense and Department of Justice.

ABSTRACT Recent works have demonstrated Filter Bank Multicarrier Spread Spectrum (FBMC-SS) to be a robust communication scheme in the presence of high-power interferers. Existing FBMC-SS symbol detector designs based on analysis filter banks (AFB) suggest using an optimal combining scheme to suppress the interferers, necessitating some noise/interference power estimation method. In this paper, we introduce a symbol detector with blind interference suppression by extending a recently developed packet detection method. We then provide an analysis to show that the existing AFB-based symbol detector and the one proposed in this paper are equivalent in typical usage scenarios. A fully-fledged receiver design is proposed utilizing this symbol detector, with specifics presented for estimation of the channel impulse response and carrier frequency offset (CFO). We also outline a method of iterating upon the channel and CFO estimations to improve the quality of both parameters. Moreover, a modification to allow improved performance of the symbol detector at high SNR is provided. Finally, simulated performance results are presented to corroborate these findings and demonstrate the efficiency of this receiver design.

INDEX TERMS Filter bank multicarrier, interference suppression, receivers, spread spectrum communication.

I. INTRODUCTION

THE DIRECT sequence spread spectrum (DS-SS) and frequency hopping spread spectrum (FH-SS) are two classical spread spectrum methods that were originally developed to establish interference-resistant communications. Early development of these methods started in the 1950s and reached a level of maturity by the early 1980s; see [1] and references therein. Multicarrier spread spectrum (MC-SS) systems were proposed and widely studied in the 1990s; see [2] and references therein. While most of the MC-SS systems make use of the celebrated orthogonal frequency division multiplexing (OFDM) for signal spreading across frequency/subcarriers, a few researchers, [3]–[5], have noted that the use of filter banks for signal spreading may lead to a robust system with higher resistance to interference. When a strong interfering signal occupies a portion of the transmission band, the filter bank's unique ability to isolate portions of the band become instrumental in rejecting the interfered part of the spectrum without affecting the non-interfered parts of it.

More recently, our team has revisited filter bank multicarrier spread spectrum (FBMC-SS) systems and explored their implementation details, [6]. In this implementation, each data packet comes with a known preamble which is used to extract the relevant channel state information (CSI), including the interference level at different subcarrier bands. The CSI is then used to set up the receiver for optimum detection of the data portion of the packet through an analysis filter bank (AFB), [7]. Among the many challenges that were faced in this development, successful detection of the preamble of each packet, by far, seemed to be the most challenging problem. The presence of high-power interference that may congest portions of the spectrum can make the task of packet detection difficult. Hence, a conventional packet detector, e.g., [8]–[11], that relies on a standard matched filter may exhibit poor performance characteristics in such

a scenario. Fortunately, the very particular form of FBMC-SS signal construction allows one to develop a modified matched filter that rejects strong interferers while performing the matched filtering operation. The proposed detector that has been named the normalized matched filter (NMF) was first presented in [12]. In this work, the NMF was used for packet detection only, and data detection was left to an AFB processing block.

The goal of this paper is to further develop the NMF of [12] to implement a complete receiver system without resorting to an AFB. The proposed system is called the NMF-based receiver, to be distinguished from the existing systems that we refer to as AFB-based receivers. As part of this development, we first design a new preamble that significantly improves the detection of the CSI. The estimated CSI includes the channel impulse response and possibly the distribution of noise plus interference across the band of transmission. In addition, our study covers the impact of carrier frequency offset (CFO) on the receiver performance, and introduces a method that allows for joint fine-tuning of the estimated channel impulse response and CFO in an iterative manner. Moreover, through computer simulations, we show that the NMF-based receiver can significantly outperform AFB-based receivers in certain practical scenarios. The theoretical reasoning behind this observation is also explained. We also show that an NMF-based receiver design may lead to a lower implementation complexity than its AFB-based counterpart.

A particular feature of the proposed NMF-based receiver that distinguishes it from its AFB-based counterpart is that it can operate without any knowledge of the interference level over different subcarrier bands. As will be discussed in this paper, by implementing the NMF in the frequency domain, the instantaneous signal energy over each subcarrier band may be measured and used to normalize the received signal for further processing. Since this step does not distinguish the incoming signal from the channel noise/interference, it may be referred to as a detector with *blind suppression of interference*. The AFB-based receiver, on the other hand, requires the interference level to be estimated at each subcarrier band at the beginning of a packet to set up a maximum ratio combining (MRC) block to reject the interference throughout the payload of the packet. It thus may perform poorly if the interference pattern over the transmission band changes across the packet. Contrary to this, the NMF-based receiver adapts its normalization coefficients over successive blocks of data that are processed, hence, it can tolerate a dynamic variation of interference across each packet.

It is worth noting that FBMC-SS with signal normalization over each subcarrier band was first proposed in [5]. However, the normalization method proposed in [5] assumes the packet detection/timing acquisition (PD/TA) as well as channel estimation have already been performed and normalization is applied to the analyzed signal samples at the output of the AFB. The shortfall here is that the packet detection and timing acquisition, and channel estimation in scenarios with strong partial band interferers is not a straightforward task. The NMF that is proposed in [12] and further explored here addresses this difficult problem that to our knowledge has no other solution available in the current literature. In order to distinguish between the proposed NMF in this paper with a conventional matched filter, we refer to the latter as the standard matched filter (SMF).

We further note that it is the band partitioning aspect of FBMC-SS that has made the design of NMF possible and effective. The NMF, thus, makes use of a special characteristic of FBMC-SS that is non-existent in DS-SS and FH-SS. Hence, FBMC-SS in conjunction with the NMF for PD/TA may be seen as a unique and perfect solution to communications in very harsh environments; *a property that is non-existent in other spread spectrum techniques.* It allows reliable communications in situations where an interferer is many tens of decibels above the spread spectrum signal level, as long as some portion of the transmission band remains interference-free. Beyond its applicability to dynamic spectrum access mentioned above, another application where FBMC-SS has been found to be effective is in communication through skywave HF channels, where electromagnetic wave reflections from layers of ionosphere may be used to establish communications over hundreds or even thousands of miles, [13], [14]. HF channels, in particular, are characterized by many narrowband interferers that could be easily rejected in a FBMC-SS receiver to achieve a near-optimum performance.

Another point which is worth noting here is that the conventional method of dealing with colored noise in most of the signal processing systems (including, communications, radar, sonar, and speech processing) is to apply a noise-whitening filter to the input signal prior to any detection process, e.g., see [15]–[21]. Such noise-whitening filters require the exclusive knowledge of the noise power spectral density (PSD) and are designed to equalize the noise PSD across the band of interest. In many wireless communication applications, the receiver has no such prior knowledge of the noise PSD and must perform estimation to resolve the noise-whitening filter. Some adaptive methods are discussed in [22]–[25] for DS-SS systems, wherein an adjustable time domain filter is applied to the receiver input in order to reduce the effect of the interferer(s). More recent works suggest suppressing the interference via transform domain methods. The techniques given in [26]–[28] apply an FFT to the received DS-SS signal and the frequency bins determined to contain interference are either attenuated or removed completely. To differentiate between an actual interfering signal and peaks in the noise floor for these approaches, some threshold estimation is required, adding further complexity. Similar methods using wavelet decomposition for DS-SS may be found in [29], and for FH-SS in [30].

The NMF-based receiver of this work implements an approximation to the noise-whitening filter in a blind fashion as an integrated part of its matched filtering process. This, at least in part, is done without any prior knowledge of the

power spectral density of the channel noise, and requires no additional adaptive methods or threshold setting. Rather than equalizing the noise power across the band of interest, in its simpler form that is presented in [12], the NMF normalizes the signal-plus-noise energy over each subcarrier band of the FBMC-SS to unity. This process greatly simplifies the matched filtering process without requiring separation of noise from the underlying signal. This implementation converges to a cascade of noise-whitening filter and matched filter in low (negative) SNR regime, where signal plus noise energy may be approximated by noise energy only. It is in light of this difference that we have avoided the noise-whitening terminology in referring to the proposed matched filter in this paper.

The rest of this paper is organized as follows. A brief review of the FBMC-SS method and the NMF are presented Sections II and III, respectively. The receiver setup for detection of the payload part of the packet, viz., the NMF-based receiver, is presented in Section IV. In Section V, a theoretical analysis that compares the performance of the proposed NMF-based receiver with its AFB-based counterpart is presented. Section VI is devoted to a novel preamble design based on Zadoff-Chu sequences and the associated packet detection method, timing acquisition, CSI estimation, and CFO detection. Simulation results that corroborate our theoretical findings are presented in Section VII. The complexity required to implement the receiver of this work compared to existing designs is discussed in Section VIII. Finally, we conclude in Section IX.

Notations: Our presentation is a mix of continuous-time and discrete-time signals. We use $x(t)$ when reference is made to a continuous-time signal, and $x[n]$ when referring to a discrete-time signal. Continuous-time formulations are adopted for presentation of the fundamental concepts and theoretical analysis in Section II through V. We then switch to discrete-time formulations to provide insight to the detailed implementation of the relevant signal processing algorithms in Section VI. Scalars are upper- and lower-case non-bold letters. Arrays are bold lower-case letters and represented as column vectors. Matrices are bold upper-case letters. The superscripts $(\cdot)^*$, $(\cdot)^{\mathrm{T}}$ and $(\cdot)^{\mathrm{H}}$ represent complex conjugate, transpose, and Hermitian transpose, respectively. The notations $\mathbb{E}[\cdot]$, $\Re[\cdot]$, and $\Im[\cdot]$ refer to statistical expectation, real part, and imaginary part of a variable, respectively. We use $\mathbf{I}$ to denote the identity matrix.

II. FILTER BANK MULTICARRIER SPREAD SPECTRUM

A. TRANSMITTER

An FBMC-SS signal, $x(t)$, is synthesized by passing the data signal

$$s(t) = \sum_n s[n]\delta(t - nT_s) \tag{1}$$

where $s[n]$ is the sequence of data symbols and T_s is the symbol duration, through a multi-band pulse-shaping filter $g(t)$. That is,

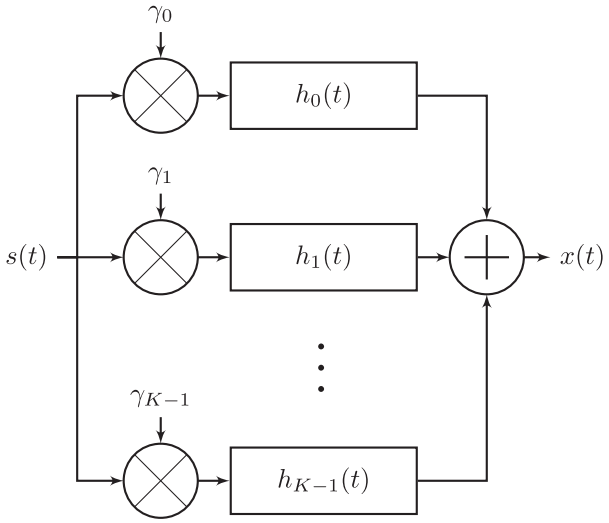

FIGURE 1. FBMC-SS transmitter, synthesis filter bank (SFB).

$$x(t) = s(t) \star g(t). \tag{2}$$

The multi-band pulse-shaping filter $g(t)$ may be expressed as

$$g(t) = \sum_{k=0}^{K-1} \gamma_k h_k(t) \tag{3}$$

where

$$h_k(t) = h(t)e^{j2\pi f_k t}. \tag{4}$$

Here, $h(t)$ is a prototype filter which determines the spectral footprint of each subcarrier. There are K subcarriers, and f_k are the subcarrier center frequencies. Subcarriers are assigned individual complex-valued spreading gains γ_k with unit magnitude, i.e., $|\gamma_k| = 1$.

The transmit signal (2) is typically generated using a synthesis filter bank (SFB), as depicted in Fig. 1. The data signal $s(t)$ is divided into K parallel branches, multiplied by spreading gains γ_k, and filtered by the subcarrier component filters $h_k(t)$ of $g(t)$. This transmitter structure can be implemented efficiently in discrete-time using a poly-phase structure as in [31, Sec. 5.4-5.5] and [32, Sec. 4.3].

B. RECEIVER

Existing literature pertaining to FBMC-SS receivers rely on an AFB structure for symbol detection. The AFB is presented in Fig. 2. An estimate of the transmit sequence is generated by passing the received signal through a bank of filters matched to each subcarrier, multiplying each branch by some combining coefficient w_k, and summing all of the branches together. Thus, the AFB-based receiver output may be expressed as

$$\hat{s}_{\mathrm{AFB}}(t) = \sum_{k=0}^{K-1} w_k h_k^*(-t) \star y(t). \tag{5}$$

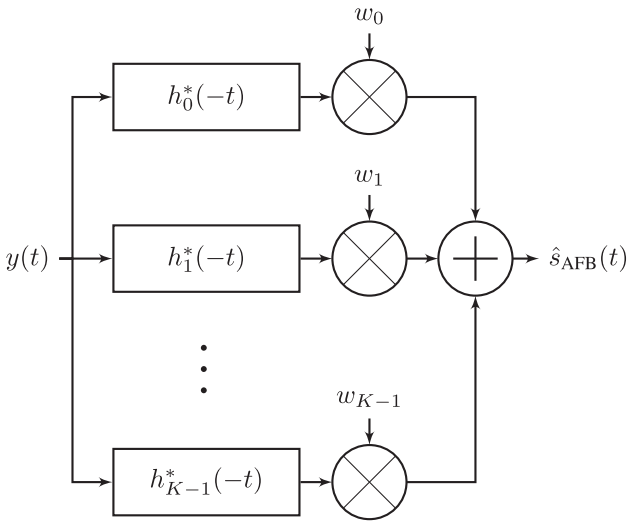

FIGURE 2. FBMC-SS receiver, analysis filter bank (AFB).

This receiver structure may also be implemented efficiently in discrete-time using a poly-phase structure as in [31, Sec. 5.4-5.5] and [32, Sec. 4.3].

III. NORMALIZED MATCHED FILTER

In digital communications, it is typical to use a filter at the receiver which is matched to the transmit pulse-shaping filter. In the case of FBMC-SS, such a matched filter collects and coherently adds the signals from all subcarrier bands. Current literature pertaining to FBMC-SS utilizes the output of the matched filter for packet detection and timing acquisition only. The task of information recovery is then performed via an AFB, as noted above, a maximum ratio combiner (MRC), [6], and possibly a RAKE receiver [13].

As mentioned in the introduction, we follow [12] and refer to the FBMC-SS matched filter without power normalization as the standard matched filter (SMF). Such an SMF has an impulse response which is the time-reversed and conjugate of (3). That is,

$$g_{\text{SMF}}(t) = g^*(-t). \tag{6}$$

The NMF extends the SMF by cascading it with a normalization filter, $q(t)$, which normalizes the output power in each subcarrier band before adding them together. This operation may be represented as

$$g_{\text{NMF}}(t) = g^*(-t) \star q(t). \tag{7}$$

In the frequency domain, (7) converts to

$$G_{\text{NMF}}(f) = G_{\text{SMF}}(f)Q(f). \tag{8}$$

The power normalization filter $Q(f)$ has a flat gain over each subcarrier band. Mathematically, this is expressed as

$$Q(f) = \sum_{k=0}^{K-1} q_k \Pi(f - f_k) \tag{9}$$

where q_k is the power normalization coefficient for the k-th subcarrier band, and

$$\Pi(f) = \begin{cases} 1, & |f| < \frac{1}{T_s}, \\ 0, & \text{otherwise.} \end{cases} \tag{10}$$

Here, following [12] (and our previous works on FBMC-SS, e.g., [6]), it is assumed that $h(t)$ is a square-root raised-cosine filter with roll-off factor $\alpha = 1$. Hence, it spans over a bandwidth of $2/T_s$, signified by $|f| < \frac{1}{T_s}$ in (10).

The power normalization coefficients q_k are calculated as

$$q_k = \frac{1}{\sigma_{y_k}} \tag{11}$$

where

$$\sigma_{y_k} = \sqrt{\frac{T_s}{2} \int_{f_k - 1/T_s}^{f_k + 1/T_s} |Y(f)|^2 \, df}. \tag{12}$$

By implementing the NMF with frequency domain filtering techniques, following the suggestion of [12], the calculation of (12) and creation of the normalization filter (9) becomes a trivial task.

IV. NMF-BASED RECEIVER STRUCTURE

In this section, we introduce a complete receiver structure that manipulates the signal output of the SMF/NMF to obtain an estimate of the transmitted information. In a later part of this paper, we show that while a receiver based on the SMF is sub-optimum when narrowband interference is present, a receiver that is built based on the NMF has a near-optimum performance.

To dig into the details of the matched filter receivers, we begin with exploring an SMF-based receiver. Also, to keep the discussion simpler, we consider the case of an additive white Gaussian noise (AWGN) channel. In this simple case, the impulse response between the transmitter input and the output of the SMF at the receiver may be expressed as

$$\eta(t) = g(t) \star g^*(-t). \tag{13}$$

The impulse response $\eta(t)$ has been explored in [6]. It has been found that at time $t = 0$, the data symbol copies from all the subcarriers (i.e., the FBMC-SS chips) are time and phase aligned and are thus added constructively. Hence, the full processing gain of the FBMC-SS is realized when the output of the SMF is sampled at the middle points of the $\eta(t)$ pulses associated with transmitted data symbols and the results are passed to the channel decoder. In the presence of a multi-path channel

$$c(t) = \sum_{i=0}^{N_{c_i}-1} c_i \delta(t - \tau_i) \tag{14}$$

where c_i are path gains and τ_i are path delays, the combined impulse response of the channel with the transmitter pulse-shaping filter, $g(t)$, and the receiver SMF, $g^*(-t)$, will be

$$\eta_c(t) = \sum_i c_i \eta(t - \tau_i). \tag{15}$$

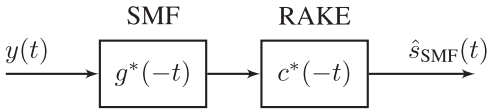

FIGURE 3. SMF-based receiver.

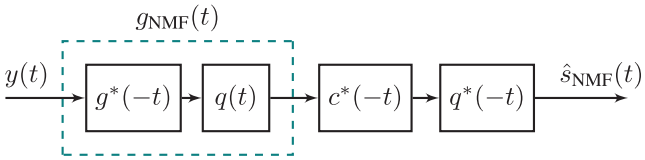

FIGURE 4. NMF-based receiver.

This result shows that for each transmitted data symbol, multiple copies of it appear at the SMF output. Obviously, the multiple copies of the data symbols can be added together constructively through a RAKE filter whose impulse response is $c^*(-t)$. This leads to the receiver structure presented in Fig. 3.

The above receiver development is also applicable to the case where the SMF is replaced by the NMF, leading us to the receiver structure presented in Fig. 4. In addition to the RAKE filter $c^*(-t)$, we include a filter matched to the power normalization step of the NMF, such that the receiver may recollect the symbol energy spread over time by $q(t)$. This additional filter allows the NMF-based receiver to match the performance realized by the AFB-based receiver with the optimal MRC. Further details are given in the next section.

A point to note here is that according to (9), the power normalization filter $q(t)$ is a zero-phase one. Hence, the cascade of $g(t)$ and $g_{\mathrm{NMF}}(t)$, similar to the cascade of $g(t)$ and $g_{\mathrm{SMF}}(t)$, at $t = 0$, leads to a sample value that is obtained by constructively adding the contributions from all the symbol chips. The difference between the SMF and NMF outputs is that while the former gives equal weight to all the symbol chips, the latter adds the symbol chips together with different weights. Accordingly, the chips with higher level of noise/interference are given a lower weight. This approach clearly suppresses the signals from the interfered subcarrier bands, hence, leads to a receiver with superior performance. It should be also noted that the normalization performed by the NMF that has been presented in [12] and summarized in Section III is only near optimum at very low SNR values. In Section VI, where we present a detailed implementation of the NMF-based receiver, we also discuss a modification to NMF that leads a near optimum performance over the full range of SNR values.

V. EQUIVALENCE OF NMF-BASED AND AFB-BASED RECEIVERS

In this section, we provide theoretical analysis to show that the NMF-based and AFB-based receivers can be expressed as equivalent forms. We take note that the transmitted signal is distorted by a multipath channel $c(t)$ and additive noise plus narrow-band interferers, denoted by $v(t)$, are added to the channel output. The subcarrier bandwidth is selected based on the expected delay spread of the channel response such that a frequency-flat approximation over each subcarrier band will be valid. This way, the channel response may be combined with the pulse-shaping filter (3), leading to the received signal

$$y(t) = s(t) \star \sum_{k=0}^{K-1} \gamma_k C_k h_k(t) + v(t). \tag{16}$$

Coefficients C_k arise from the equivalent baseband response of the channel at the k-th subcarrier, [6].

A. AFB-BASED RECEIVER

When the received signal (16) is passed through the AFB, the output of the k-th subcarrier filter before combining is

$$z_{\mathrm{AFB},k}(t) = w_k h_k^*(-t) \star \left(s(t) \star \sum_{k'=0}^{K-1} \gamma_{k'} C_{k'} h_{k'}(t) + v(t) \right). \tag{17}$$

Because of the non-overlapping subcarriers in FBMC-SS, we may disregard all $k' \neq k$, hence,

$$\begin{aligned} z_{\mathrm{AFB},k}(t) &= w_k h_k^*(-t) \star (s(t) \star \gamma_k C_k h_k(t) + v(t)) \\ &= w_k \big(s(t) \star \gamma_k C_k h_k'(t) + v_k'(t) \big), \end{aligned} \tag{18}$$

where $h_k'(t) = h_k(t) \star h_k^*(-t)$. We assume the subcarrier filter response is normalized such that $|h_k'(0)| = 1$. The filtered noise term $v_k'(t)$ arises from the noise plus interference $v(t)$ after passage through $h_k^*(-t)$.

The AFB-based receiver output after combining is given by

$$\hat{s}_{\mathrm{AFB}}(t) = \sum_{k=0}^{K-1} z_{\mathrm{AFB},k}(t). \tag{19}$$

To maximize the SNR observed at the output of the receiver, the MRC technique, e.g., see [6], is applied. This leads to the combining coefficients

$$w_k = \frac{\gamma_k^* C_k^* / \sigma_{v',k}^2}{\sum_{k=0}^{K-1} |C_k|^2 / \sigma_{v',k}^2}. \tag{20}$$

Using these coefficients, the phase contributions of γ_k and C_k are removed, hence, the information symbols from different subcarrier bands are added constructively. The summation in the denominator of (20) is a scaling constant that may be removed when the transmitted data symbols belong to a constant modulo constellation, e.g., a BPSK (binary phase

shift keying) or a QPSK (quadrature phase-shift keying) constellation. Here, we assume this is the case and drop this constant in the following equations.

Dropping the denominator part in (20), and substituting the result in (19), we get

$$\hat{s}_{\mathrm{AFB}}(t) = \sum_{k=0}^{K-1} \left(s(t) \star \frac{|C_k|^2}{\sigma^2_{\nu',k}} h'_k(t) + \gamma_k^* \frac{C_k^*}{\sigma^2_{\nu',k}} \nu'_k(t) \right). \quad (21)$$

B. NMF-BASED RECEIVER

Using the NMF-based receiver architecture given in Fig. 4, one finds that

$$\hat{s}_{\mathrm{NMF}}(t) = q^*(-t) \star c^*(-t) \star q(t) \star g^*(-t) \star (c(t) \star x(t) + \nu(t)). \quad (22)$$

Applying the Fourier transform to both sides of (22), we get

$$\hat{S}_{\mathrm{NMF}}(f) = \bar{S}_{\mathrm{NMF}}(f) + V_{\mathrm{NMF}}(f), \quad (23)$$

where

$$\bar{S}_{\mathrm{NMF}}(f) = |Q(f)|^2 |C(f)|^2 |G(f)|^2 S(f) \quad (24)$$

is the part that originates from the transmitted signal, and

$$V_{\mathrm{NMF}}(f) = |Q(f)|^2 C^*(f) G^*(f) V(f) \quad (25)$$

is the part that originates from the channel noise plus interference.

Recalling (3) and (4), one will find that

$$\begin{aligned} \bar{S}_{\mathrm{NMF}}(f) &= S(f)|Q(f)|^2 |C(f)|^2 \sum_{k=0}^{K-1} |\gamma_k|^2 |H_k(f)|^2 \\ &= S(f) \sum_{k=0}^{K-1} q_k^2 |C_k|^2 |H_k(f)|^2 \end{aligned} \quad (26)$$

where the second line follows from the flat gain assumption over each subcarrier band and the fact that $Q(f)$ is a constant equal to q_k over the k-th subcarrier band. Applying the inverse Fourier transform to both sides of (26), we get

$$\bar{s}_{\mathrm{NMF}}(t) = s(t) \star \sum_{k=0}^{K-1} q_k^2 |C_k|^2 h'_k(t). \quad (27)$$

The noise component (25) can be decomposed following the same method of subcarrier separation, to obtain

$$V_{\mathrm{NMF}}(f) = \sum_{k=0}^{K-1} q_k^2 C_k^* \gamma_k^* V'_k(f) \quad (28)$$

where $V'_k(f) = H_k^*(f) V(f)$. Applying the inverse Fourier transform to both sides of (28), we get

$$\nu_{\mathrm{NMF}}(t) = \sum_{k=0}^{K-1} q_k^2 C_k^* \gamma_k^* \nu'_k(t). \quad (29)$$

Combining the result in (27) and (29) and rearranging the result, we obtain

$$\hat{s}_{\mathrm{NMF}}(t) = \sum_{k=0}^{K-1} \left(s(t) \star q_k^2 |C_k|^2 h'_k(t) + q_k^2 C_k^* \gamma_k^* \nu'_k(t) \right). \quad (30)$$

Now, comparing (30) and (21), one may find that there is a great level of similarity in $\hat{s}_{\mathrm{AFB}}(t)$ and $\hat{s}_{\mathrm{NMF}}(t)$, though some key differences may be seen. The weighting coefficient $|C_k|^2/\sigma^2_{\nu',k}$ in (21) is replaced by $q_k^2|C_k|^2$ in (30). Recalling (11), one may find that while the AFB-based receiver uses a power normalization which is determined by the noise plus interference power only, the NMF-based receiver applies a power normalization based on the signal, interference, and noise at each subcarrier band. The difference between the two receivers will thus become negligible at lower level of SNR (say, below -10 dB). Hence, recalling that FBMC-SS is targeted to operate at such low SNR values, the receiver outputs $\hat{s}_{\mathrm{AFB}}(t)$ and $\hat{s}_{\mathrm{NMF}}(t)$ will be effectively the same. As the SNR increases, the NMF-based receiver may begin to show some performance degradation compared to the AFB-based receiver. In the next section, we will show how this shortcoming of the NMF-based receiver may be fixed.

VI. NMF-BASED RECEIVER DETAILS

With the basic NMF-based receiver structure introduced in the preceding section, here, we present a detailed implementation of such a receiver. Before we dive into the details of our proposed receiver, we recall that in packetized data transmission, each packet starts with a preamble that consists of a sequence of pilot symbols which are known to the receiver. In some of the earlier implementations of FBMC-SS, e.g., [7], the first segment of preamble consists of a sequence of alternating BPSK symbols. Once passed through the matched filter, a periodic series of peaks with alternating phase will appear at the output. The receiver assumes a packet is present when a number of such peaks occurs at the same timing phase over a handful of symbols. This first segment of the preamble may be also used to obtain a coarse estimation of carrier frequency offset (CFO) which will be then removed from the remaining part of the received signal. The NMF was introduced later to improve PD/TA performance with this preamble structure in mind, [12]. An estimate of the channel is then obtained after passing the time-aligned preamble signal into an AFB and matching its outputs with a second segment of the preamble. This second segment may be any arbitrary pseudo random sequence.

In this paper, we adopt a Zadoff-Chu (ZC) sequence for the second segment of the preamble. We show that this choice, when used along with the NMF, leads to an effective receiver design. First, by taking advantage of the autocorrelation property of ZC sequences, we show that an accurate estimate of the channel impulse response can be obtained trivially. Second, we examine the impact of any residual CFO (that may remain after removing its coarse estimate) on the

estimated channel. Third, by making use of the channel estimate, we develop an optimal estimator to obtain an accurate estimate of the residual CFO. Finally, to obtain a more accurate estimate of the channel, we propose re-estimating the channel after removal of the residual CFO from the received signal.

Fig. 5 presents a block diagram of the receiver that was outlined above. The portion appearing to the left of the NMF block has been addressed in some previous works, e.g., [7], hence, is not discussed here. The rest of the receiver blocks, after the NMF, extensively make use of the properties of the ZC sequence to design an effective channel estimator as well as a method of obtaining any residual CFO that may have remained after the coarse CFO correction which occurs before the NMF. We assume the residual CFO, here, is *sufficiently small* to warrant satisfactory operation of the proposed receiver design. A range that quantifies the term "sufficiently small CFO" will be given in a later part of this section. The reader may note that the coarse estimate of the CFO, prior to $g_{\text{NMF}}(t)$, and the fine estimate of residual CFO, after $g_{\text{NMF}}(t)$, are represented by $\widehat{\Delta}_f$ and $\hat{\delta}_f$, respectively.

The rest of this section is organized as follows. In Section IV-A, we develop some theoretical results that reveal the basic properties of the ZC sequence in relation to the proposed NMF-based receiver. These results are then used to develop an optimum channel impulse response (CIR) estimator, in Section IV-B. Section IV-C is devoted to a study of the impact of the residual CFO on the estimated CIR. The finding in Sections IV-B and IV-C are made use of in Section IV-D to propose an optimum estimator for the residual CFO. Section IV-E outlines a method of iterating upon the channel and CFO estimators to obtain improved estimates of both terms. Finally, a modification to the symbol detector is discussed in Section IV-F to enable optimal performance of the NMF at high SNR values.

A. ZC SEQUENCE AND INDUCED RESULTS

For the second portion of preamble, we propose using multiple periods of a ZC sequence of length Z. Here, without any loss of generality, we assume Z is an even number and consider a root-1 ZC sequence expressed as in [33], [34].

$$a[n] = e^{-j\pi n^2/Z} \qquad \text{for } 0 \le n < Z-1 \tag{31}$$

We also define the continuous-time equivalent of the ZC sequence $a[n]$ as

$$a(t) = \sum_{n=0}^{Z-1} a[n]\delta(t - nT_s). \tag{32}$$

Repeating multiple periods of $a(t)$ and pulse-shaping the result, following (1) and (2), leads to a preamble signal that we refer to as $x_{\text{ZC}}(t)$. After passing through the channel, the received signal is

$$y_{\text{ZC}}(t) = c(t) \star x_{\text{ZC}}(t) + v(t), \tag{33}$$

where $v(t)$ is the noise plus interference. This leads to the NMF output of

$$y_{\text{NMF}}(t) = g^*(-t) \star q(t) \star (c(t) \star x_{\text{ZC}}(t) + v(t)). \tag{34}$$

Next, we define

$$p(t) = a^*(-t) \star g^*(-t) \star q(t) \star (c(t) \star x_{\text{ZC}}(t) + v(t)) \tag{35}$$

and note that this is effectively the correlation between $y_{\text{NMF}}(t)$ and one period of the ZC preamble. We also make use of the zero-autocorrelation property of ZC sequences, [33], [34], to simplify the right-hand side of (35). This property states that the circular convolution of $a[n]$ by its time reversed and conjugated version has a value of Z at the zero lag, and is equal to zero otherwise.

Recalling that $x_{\text{ZC}}(t)$ is periodic in its steady state part, straightforward manipulations of (35) reveals that such a period of $p(t)$ has the form of

$$p_0(t) = Z\tilde{\eta}(t) \circledast \tilde{q}(t) \circledast \tilde{c}(t) + \zeta(t), \tag{36}$$

where $\tilde{\eta}(t)$, for $0 \le t < ZT_s$, is a single period of the periodic version of $\eta(t)$ expressed as $\sum_n \eta(t - nZT_s)$, and $\tilde{q}(t)$ and $\tilde{c}(t)$ are defined similarly. Moreover, $\zeta(t)$ is the respective noise term.

The combined impulse response $\eta(t) = g(t) \star g^*(-t)$ has been studied in [6], wherein, it has been found that this response may be described as a series of narrow sinc pulses multiplied by the Nyquist pulse $h(t) \star h(-t)$. The inclusion of the power normalization filter $q(t)$ reduces the amplitude of these sinc pulses and make them wider over time. Nevertheless, recalling that $q(t)$ is zero-phase, the basic form of $\eta(t)$ remains unchanged. When $h(t)$ is a square-root raised-cosine pulse-shape with roll-off factor $\alpha = 1$ and the subcarrier center frequencies are spaced at $2/T_s$ Hz apart, as in [6], $\eta(t)$ and, hence, $\eta(t) \star q(t)$ can be approximated by a series of 3 impulses as

$$\eta(t) \star q(t) \propto 2\beta K(\delta(t) - 0.5\delta(t \pm T_s/2)) \tag{37}$$

where $\propto$ denotes proportional to. In (37), the sinc pulses are approximated by the Dirac delta function, $\delta(t)$, following the identity $\delta(x) = \lim_{\varepsilon \to 0} \frac{\sin(x/\varepsilon)}{\pi x}$, [35]. Moreover, the coefficient $2K$ is added to indicate the processing gain that arises from the matched filtering operation $g^*(-t)$, and β is an attenuation factor caused by the power normalization filter $q(t)$.

Substituting (37) in (36), we get

$$p_0(t) = 2\beta KZ(c(t) - 0.5c(t \pm T_s/2)) + \zeta(t). \tag{38}$$

The extra factor Z on the right-hand side of (38), compared to (37), reflects the processing gain arising from the matched filtering operation with $a^*(-t)$.

Assuming the delay spread of the channel is small compared to the symbol interval T_s, one may note that the three impulse responses that appear on the right-hand side of (38) constitutes a short span of each period of the preamble. This observation, along with the fact that the combination of the

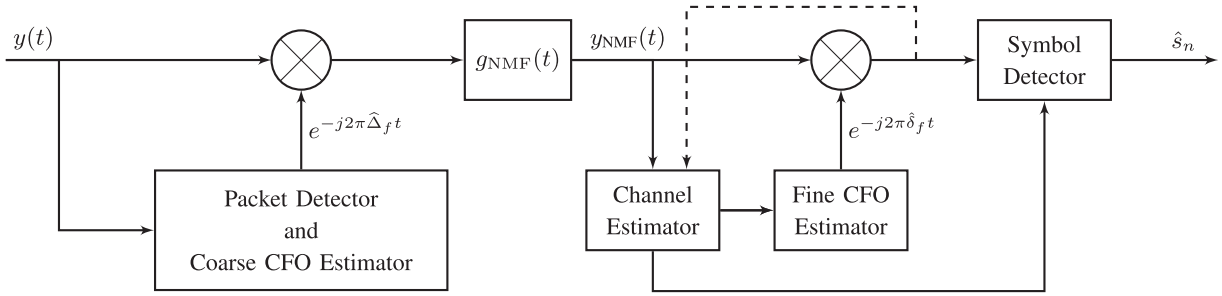

FIGURE 5. Block diagram of the proposed NMF-based receiver.

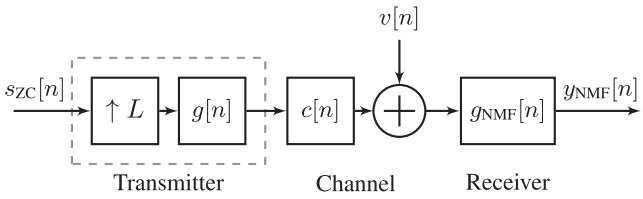

FIGURE 6. Discrete time NMF-based transceiver. Only the front portion of the receiver is shown.

two matched filtering steps $g^*(-t)$ and $a^*(-t)$ results in a processing gain $2KZ$, should expectedly lead to an accurate estimate of the channel. Obviously, this estimate improves as K and Z increase.

B. CHANNEL ESTIMATION

To cast the above development in a form that facilitates an optimum estimation of the channel impulse response, we begin with the discrete-time system block diagram of an FBMC-SS transceiver that is presented in Fig. 6. Here, concentrating on the ZC portion of preamble, the input to the transmitter is a periodic ZC sequence $s_{\mathrm{ZC}}[n]$ with Z samples per period; a period of $s_{\mathrm{ZC}}[n]$ is $a[n]$, defined in (31). The expander parameter L indicates the number of signal samples per symbol interval T_s. The pulse-shaping filter $g[n]$, the channel $c[n]$, the NMF $g_{\mathrm{NMF}}[n]$ and its output $y_{\mathrm{NMF}}[n]$, and the additive noise $v[n]$ are the discrete-time versions of the corresponding continuous-time functions that were defined earlier. It should be also noted that prior to $s_{\mathrm{ZC}}[n]$ comes the first part of the preamble that is used for packet detector and coarse carrier recovery, e.g., [12], [36]; also see Fig. 5. We have removed these details in Fig. 6.

As discussed above, if $y_{\mathrm{NMF}}[n]$ is passed through a filter matched to the ZC sequence, the periodic repetitions of triple replicas of the channel impulse response expressed as in (38) will appear at the output. A period of $y_{\mathrm{NMF}}[n]$, starting with a sample that corresponds to the starting point of the triple channel impulse responses, is extracted to be used for channel estimation as explained in the sequel. The samples of the extracted period of preamble are stored in a column vector that is denoted as $\mathrm{y}_{\mathrm{NMF}}$. We also note that $\mathrm{y}_{\mathrm{NMF}}$ has a length of $N_{\mathrm{pr}} = Z \times L$.

Next, we note that the vector $\mathrm{y}_{\mathrm{NMF}}$ may be presented as

$$\mathrm{y}_{\mathrm{NMF}} = \mathrm{QG}^*\mathrm{CGEs}_{\mathrm{ZC}} + \mathrm{QG}^*\mathrm{v}. \tag{39}$$

Here, s_{ZC} is a column vector of length Z representing a period of the ZC sequence $s_{\mathrm{ZC}}[n]$, and $\mathbf{E}$ is an expander matrix that inserts $L-1$ zeros after each element of s_{ZC}, resulting in a vector of length N_{pr}. This vector is then multiplied by the circulant matrix $\mathbf{G}$ corresponding to the pulse-shaping filter $g[n]$. The first column of $\mathbf{G}$ is obtained by taking the samples of $g[n]$, extending them to a length N_{pr} by appending sufficient zeros to the end, and circularly shifting the result so that the middle sample of $g[n]$ will be the first/zeroth sample of the final result. This produces a column vector of the zero-phase version of the pulse-shaping filter. The circulant matrix $\mathbf{G}$ is then constructed accordingly. The matrix $\mathbf{C}$ is a circulant matrix whose first column is the channel impulse response extended to the length N_{pr} by appending zeros to its end. The final operation on the right-hand side of (39), i.e., multiplication by QG^*, signifies the NMF step at the receiver. Here, we note that since $\mathbf{G}$ corresponds to a zero-phase version of $g[n]$, its matched version is simply G^*. The circulant matrix $\mathbf{Q}$ is constructed similarly.

To proceed, we recall that a circulant matrix $\mathbf{A}$ may be decomposed following [37, Sec. 3.1] as

$$\mathrm{A} = \boldsymbol{\mathcal{F}}^{-1}\mathrm{A_f}\boldsymbol{\mathcal{F}} \tag{40}$$

where $\boldsymbol{\mathcal{F}}$ is the normalized DFT matrix such that $\boldsymbol{\mathcal{F}}^* = \boldsymbol{\mathcal{F}}^{-1}$, and $\mathrm{A_f}$ is a diagonal matrix whose diagonal elements are the DFT of the first column of $\mathbf{A}$. Making use of (40) and following a similar notation to expand all the circulant matrices in (39) and finally applying the DFT to both sides of the result, we obtain

$$\mathrm{y}_{\mathrm{NMF,f}} = \mathrm{Q_f G_f^* C_f G_f s}_{\mathrm{ZC,f}} + \mathrm{Q_f G_f^* v_f} \tag{41}$$

Here, $\mathrm{s}_{\mathrm{ZC,f}}$ and $\mathrm{v_f}$ denote the DFTs of the length N_{pr} vectors $\mathrm{Es}_{\mathrm{ZC}}$ and v, respectively. We note that (41) may be rearranged as

$$\mathrm{y}_{\mathrm{NMF,f}} = \mathrm{Q_f G_f^* G_f S}_{\mathrm{ZC,f}}\mathrm{c_f} + \mathrm{Q_f G_f^* v_f} \tag{42}$$

where $\mathrm{S}_{\mathrm{ZC,f}}$ is the diagonal matrix obtained by taking the elements of $\mathrm{s}_{\mathrm{ZC,f}}$ as its diagonal elements.

Next, we define the length L_c vector c, which contains the samples of the channel impulse response $c(t)$. Also, for convenient formulations, it is assumed that the path delays τ_i are integer multiples of the sampling interval. Moreover, taking note that for typical channels, $L_c < N_{\text{pr}}$,

$$\mathrm{c_f} = \boldsymbol{\mathcal{F}}_{\mathrm{p}}\mathrm{c} \tag{43}$$

where $\boldsymbol{\mathcal{F}}_{\mathrm{p}}$ is the portion of the DFT matrix obtained by taking its first L_c columns. Substituting (43) in (42), we get the linear equation

$$\mathrm{y_{NMF,f}} = \mathrm{D_f c} + \mathrm{v_f'} \tag{44}$$

where

$$\mathrm{D_f} = \mathrm{Q_f G_f^* G_f S_{ZC,f}} \boldsymbol{\mathcal{F}}_{\mathrm{p}} \tag{45}$$

is of size $N_{\text{pr}} \times L_c$, and $\mathrm{v_f'} = \mathrm{Q_f G_f^* v_f}$. We may also note that $\mathrm{y_f}$ and $\mathrm{v_f'}$ are vectors of length N_{pr}. The form of (44) allows us to directly apply the familiar estimation methods for linear models as in [38, Sec. 14.3].

Assuming that the noise samples of $\mathbf{v_f'}$ are Gaussian and the channel path gains of (14) are Rayleigh distributed, we may apply [38, Th. 10.3] to obtain the minimum mean square error (MMSE) estimate of $\mathbf{c}$ as

$$\hat{\mathbf{c}} = \left(\boldsymbol{\Sigma}_{\mathbf{cc}}^{-1} + \mathbf{D}_{\mathrm{f}}^{\mathrm{H}} \boldsymbol{\Sigma}_{\mathrm{v_f' v_f'}}^{-1} \mathrm{D_f}\right)^{-1} \mathbf{D}_{\mathrm{f}}^{\mathrm{H}} \boldsymbol{\Sigma}_{\mathrm{v_f' v_f'}}^{-1} \mathrm{y_{NMF,f}} \tag{46}$$

where Σ_{cc} and $\boldsymbol{\Sigma}_{\mathrm{v_f' v_f'}}$ are the covariance matrices of the channel and noise vectors c and $\mathrm{v_f'}$, respectively. Here, it is assumed that $\boldsymbol{\Sigma}_{\text{cc}}$ is known to the receiver. It should also be noted that the matrix inverse $\boldsymbol{\Sigma}_{\text{cc}}^{-1}$ may not exist, as is the case where the number of discrete path gains, that is, N_{c_i} in (14), is smaller than L_c. This problem may be solved trivially by adding a small regularization factor to the diagonal elements of $\boldsymbol{\Sigma}_{\text{cc}}$ before inverting. Simulated results presented in Section VII indicate that this regularization results in an insignificant loss in the estimator performance.

The following steps may be taken to simplify (46). Assuming that the receiver operates at some negative SINR across the transmission band, the normalization gain q_k across the k-th subcarrier band is dominated by the interference plus noise power. In this case, with the assumption that the interference plus noise across each subcarrier band has a flat spectrum, one will find that $\boldsymbol{\Sigma}_{\mathrm{v_f v_f}}$ is a diagonal matrix that is proportional to $\mathrm{Q_f^{-2}}$. Now, recalling that $\mathrm{v_f'} = \mathrm{Q_f G_f^* v_f}$, we find

$$\boldsymbol{\Sigma}_{\mathrm{v_f' v_f'}} = \mu \mathrm{G_f^* G_f}. \tag{47}$$

Here, μ is a constant factor whose exact value will be derived later.

Substituting (45) and (47) in (46), we get

$$\hat{\mathrm{c}} = \mu^{-1}\left(\boldsymbol{\Sigma}_{\mathbf{cc}}^{-1} + \boldsymbol{\mathcal{F}}_{\mathrm{p}}^{\mathrm{H}} \Lambda \boldsymbol{\mathcal{F}}_{\mathrm{p}}\right)^{-1} \boldsymbol{\mathcal{F}}_{\mathrm{p}}^{\mathrm{H}} \mathrm{Q_f^* S_{ZC,f}^* y_{NMF,f}} \tag{48}$$

where

$$\Lambda = \mu^{-1} \mathrm{Q_f^* Q_f G_f^* G_f S_{ZC,f}^* S_{ZC,f}}. \tag{49}$$

Note that since the matrices $\mathrm{Q_f}$, $\mathrm{G_f}$, and $\mathrm{S_{ZC,f}}$ are diagonal, Λ is also diagonal, and its diagonal elements may be obtained trivially through multiplication of diagonal elements of these matrices.

The estimation error of (48) may be defined as the difference between the obtained estimate and the actual value of $\mathbf{c}$, that is,

$$\boldsymbol{\epsilon} = \hat{\mathbf{c}} - \mathbf{c}. \tag{50}$$

The size of this estimation error is given by the expected value of the Euclidean norm of $\boldsymbol{\epsilon}$, i.e., $\mathbb{E}[\boldsymbol{\epsilon}^{\mathrm{H}}\boldsymbol{\epsilon}]$. We also recall that the MMSE of the channel estimate, i.e., the minimum value of $\mathbb{E}[\boldsymbol{\epsilon}^{\mathrm{H}}\boldsymbol{\epsilon}]$ that could be obtained, can be expressed as

$$\begin{aligned}\mathrm{MMSE} &= \mathrm{tr}\left[\boldsymbol{\Sigma}_{\hat{\mathbf{c}}\hat{\mathbf{c}}}\right] \\ &= \mathrm{tr}\left[\left(\boldsymbol{\Sigma}_{\mathbf{cc}}^{-1} + \boldsymbol{\mathcal{F}}_{\mathrm{p}}^{\mathrm{H}} \Lambda \boldsymbol{\mathcal{F}}_{\mathrm{p}}\right)^{-1}\right],\end{aligned} \tag{51}$$

following the analysis provided in [38, Ch. 10].

Finally, we provide some argument that leads to the value of the constant factor μ in (47). We recall that the FFT size used for the above processing steps is $N_{\text{pr}} = ZL$. Also, there are $L/2$ subcarriers over the transmission band. Accordingly, each subcarrier band is covered by $N_{\text{pr}}/(L/2) = 2Z$ frequency bins of the FFT output. Moreover, assuming that for a given subcarrier band, say the k-th subcarrier band, each of the corresponding elements has a power of q_k^{-2}, the total power in this band will be $\rho_k^2 = 2Zq_k^{-2}$. This along with the arguments that are given in the last few lines above (47) will lead to $\mu = 2Z$.

C. IMPACT OF RESIDUAL CFO ON THE ESTIMATED CIR

The presence of some residual CFO introduces distortion to the matched filtered signal $\mathbf{y}_{\text{NMF}}$, including the introduction of some intercarrier interference (ICI). By adding the impact of a residual CFO δ_f to the received signal, (39) modifies to

$$\mathrm{y_{NMF}} = \mathrm{Q G^* \Theta C G E s_{ZC}} + \mathrm{Q G^* v} \tag{52}$$

where Θ is diagonal matrix with elements $1, e^{j2\pi\delta_f T_s/L}, e^{j4\pi\delta_f T_s/L}, e^{j6\pi\delta_f T_s/L}, \ldots,$ along its diagonal. These, clearly, are the successive additional phase angles that are introduced by the CFO. It may be also noted that, strictly speaking, these phase angles should start with a random phase. Here, this random phase is replaced by zero leading to the first element of the above sequence being one. Moreover, careful examination of the channel estimator equations reveals that the presence of an initial phase angle adds a scalar phase gain to the estimated channel, which has no significant effect on the receiver performance. We will make use of this scalar phase gain later for estimation of the residual CFO. However, for the first part of our derivations, here, we let the initial phase of the residual CFO be zero, without any loss of generality of our observation.

Starting with (52) and following the same line of derivations that led to (48), for the present case, we find the dual

of (42) as

$$y_{NMF,f} = Q_f G_f^* \Theta_f G_f S_{ZC,f} c_f + Q_f G_f^* v_f \tag{53}$$

where $\Theta_f = \mathcal{F}\Theta\mathcal{F}^*$.

Replacement of (53) in (48) and some straightforward manipulations, leads to

$$\hat{c} = \hat{c}_0 + \boldsymbol{\epsilon}_{\mathbf{v}} \tag{54}$$

where

$$\hat{c}_0 = \left(\boldsymbol{\Sigma}_{\mathbf{cc}}^{-1} + \mathcal{F}_p^H \Lambda \mathcal{F}_p\right)^{-1} \left(\mathcal{F}_p^H \Lambda' \mathcal{F}_p\right) c \tag{55}$$

and $\boldsymbol{\epsilon}_{\mathbf{v}}$ is the error contributed by the noise term $\mathbf{v}_f'$ appearing in (44). In (55),

$$\Lambda' = \mu^{-1} S_{ZC,f}^* G_f^* Q_f^* Q_f \Theta_f G_f S_{ZC,f}. \tag{56}$$

One may note that when there is no CFO, thus, $\Theta_f = I$, (56) reduces to (49), hence, $\hat{c}_0$ approaches c as the SNR increases, i.e., as $\boldsymbol{\Sigma}_{\mathbf{cc}}^{-1}$ becomes insignificant relative to $\mathcal{F}_p^H \Lambda \mathcal{F}_p$. The presence of residual CFO will lead to an estimate of $\mathbf{c}$ that is distorted. The distortion here is characterized by the gain matrix

$$\mathcal{G} = \left(\boldsymbol{\Sigma}_{\mathbf{cc}}^{-1} + \mathcal{F}_p^H \Lambda \mathcal{F}_p\right)^{-1} \left(\mathcal{F}_p^H \Lambda' \mathcal{F}_p\right). \tag{57}$$

It turns out that an accurate analysis of (57) is hard to perform, depending critically on the specific values of the channel tap covariance matrix $\boldsymbol{\Sigma}_{\mathbf{cc}}$ and power normalization filter $\mathbf{Q}_f$. Nevertheless, numerical examples reveal that $\mathcal{G}$ is predictable within a good approximation. The observation that we have made through numerical results is that

$$\mathcal{G} \approx \varphi(\delta_f)\mathrm{sinc}(\delta_f T_s Z)\mathcal{G}_0 \tag{58}$$

where $\mathcal{G}_0$ is the gain matrix (57) when $\delta_f = 0$, $\mathrm{sinc}(x) = \frac{\sin(\pi x)}{\pi x}$, and $\varphi(\delta_f) = e^{j\pi\delta_f T_s Z}$.

Here, we quantify the accuracy of (58) by presenting some statistical results based on numerical calculations. For this purpose, we consider the case where $K = 64$, $L = 128$, and $Z = 16$. The channel covariance matrix used in these simulations matches the TDL-A model recommended by [39] with an RMS delay spread of 30 ns, and the symbol rate is $1/T_s = 250$ kHz following the FBMC-SS implementation of [7]. We also choose the diagonal elements of the power normalization matrix Q_f as a set of random numbers uniformly distributed in the range of 0 to 1. This experiment is repeated 1000 times, for different realizations of Q_f, and the results are collectively combined to present the following figures.

If the approximation (58) holds, we should expect

$$\varphi^*(\delta_f)\mathcal{G}\mathcal{G}_0^{-1} \approx \mathrm{sinc}(\delta_f T_s Z)\mathbf{I}. \tag{59}$$

Fig. 7 presents the mean of the real and imaginary parts of diagonal elements of the matrix appearing on the left-hand side of (59) (averaged over all the diagonal elements), and compares them against the approximated value $\mathrm{sinc}(\delta_f T_s Z)$ as δ_f varies. The variance of the diagonal elements as δ_f varies is presented in Fig. 8. Moreover, the variance of the set of off-diagonal elements of $\varphi^*(\delta_f)\mathcal{G}\mathcal{G}_0^{-1}$ are also presented in Fig. 8. These results that we have repeated for various choices of channel model and parameters K, L, and Z further confirm excellent accuracy of the approximation in (58).

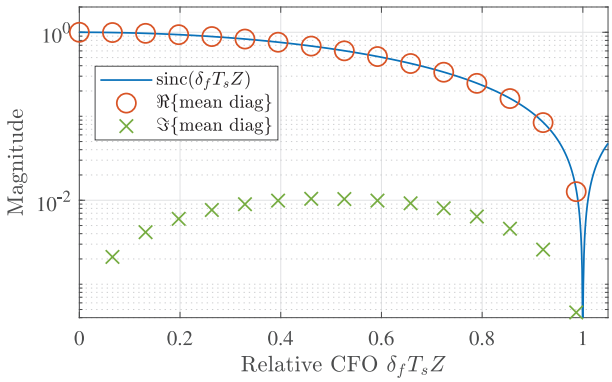

FIGURE 7. Mean of real and imaginary components of evaluated diagonal elements of (59).

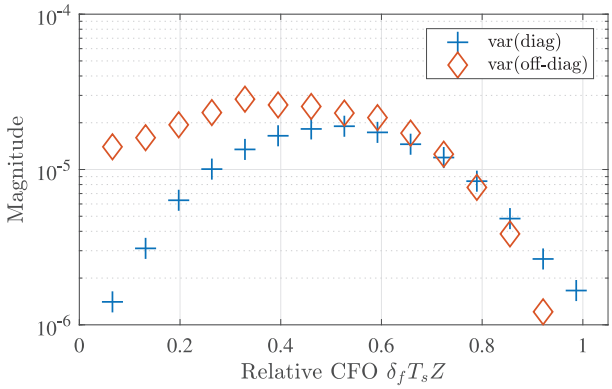

FIGURE 8. Variance of diagonal and off-diagonal elements of (59).

We take note, here, that in Fig. 8 the variance of the off-diagonal terms increases slightly with the CFO, before sharply decreasing. One might intuit that the variance of the off-diagonal terms should be strictly increasing with δ_f due to the respective increase in ICI distortion. However, this may not be true (and appears to be false as the results in Fig. 8 show), given the attenuation factor $\mathrm{sinc}(\delta_f T_s Z)$ in (58).

Using (58) in (55), one may note that

$$\hat{c}_0 \approx \varphi(\delta_f)\mathrm{sinc}(\delta_f T_s Z)\mathcal{G}_0 c \tag{60}$$

within a good approximation. It may be also noted that as SNR increases, $\mathcal{G}_0$ approaches the identity matrix, hence, c_0 approaches the exact channel response $\mathbf{c}$ within a constant factor $\varphi(\delta_f)\mathrm{sinc}(\delta_f T_s Z)$. Moreover, this constant factor approaches one as $\delta_f \to 0$. Also, one may note that to make sure this constant does not become too small, δ_f should remain with the lock range

$$-\frac{\psi}{T_s Z} < \delta_f < \frac{\psi}{T_s Z} \tag{61}$$

where ψ is some reasonable positive value smaller than 1, e.g., $\psi = 0.5$.

D. CFO ESTIMATOR

We will now introduce a method for estimation of the residual CFO δ_f by leveraging the phase difference between channel estimates obtained from two different portions of the preamble. Let us denote these two channel estimates as $\hat{\mathbf{c}}_a$ and $\hat{\mathbf{c}}_b$, where $\hat{\mathbf{c}}_a$ is estimated starting at the time index n, and $\hat{\mathbf{c}}_b$ is estimated at M symbols later, i.e., starting at the time index $n + M \times L$.

Following the notation in (54), one will find that

$$\hat{\mathrm{c}}_a = \hat{\mathrm{c}}_{a,0} + \boldsymbol{\epsilon}_a \tag{62}$$

and

$$\hat{\mathrm{c}}_b = \hat{\mathrm{c}}_{b,0} + \boldsymbol{\epsilon}_b. \tag{63}$$

Moreover, recalling that the vectors $\hat{\mathrm{c}}_{a,0}$ and $\hat{\mathrm{c}}_{b,0}$ are proportional to the channel impulse response at the respective time instances n and $n + ML$, one will find that

$$\hat{\mathrm{c}}_{b,0} = \hat{\mathrm{c}}_{a,0} e^{j2\pi\delta_f T_s M}. \tag{64}$$

Substituting (64) in (63) and then using (62), we obtain

$$\hat{\mathrm{c}}_b = \hat{\mathrm{c}}_a e^{j2\pi\delta_f T_s M} + \boldsymbol{\epsilon}_c \tag{65}$$

where $\boldsymbol{\epsilon}_c = \boldsymbol{\epsilon}_b - \boldsymbol{\epsilon}_a e^{j2\pi\delta_f T_s M}$ is the combined estimation error vector.

Next, we note that the least-squares estimate of the exponential coefficient $e^{j2\pi\delta_f T_s M}$ that results in the best match between the two channel estimates $\hat{\mathrm{c}}_a$ and $\hat{\mathrm{c}}_b$ is $(\hat{\mathrm{c}}_a^{\mathrm{H}}\hat{\mathrm{c}}_b)/(\hat{\mathrm{c}}_a^{\mathrm{H}}\hat{\mathrm{c}}_a)$. Noting that $\hat{\mathrm{c}}_a^{\mathrm{H}}\hat{\mathrm{c}}_a$ is a real and positive scalar, one may find the least-squares estimate of δ_f as

$$\hat{\delta}_f = \frac{1}{2\pi T_s M} \angle\left(\hat{\mathrm{c}}_a^{\mathrm{H}}\hat{\mathrm{c}}_b\right) \tag{66}$$

where the $\angle(x)$ denotes the angle of a complex number x.

Taking note that the unambiguous range of $\angle(\hat{\mathrm{c}}_a^{\mathrm{H}}\hat{\mathrm{c}}_b)$ is limited to the interval $-\pi$ through $+\pi$, one may realize that the CFO δ_f has a lock range of

$$-\frac{1}{2MT_s} < \delta_f < \frac{1}{2MT_s}. \tag{67}$$

This range matches with (61) if $M = Z$ and $\psi = 0.5$. It should be further noted that because of reasons mentioned prior to (61), even if M is chosen smaller than Z, the lock range (61) should be still adhered to.

E. ITERATIVE CHANNEL AND CFO ESTIMATION

The observations made above is that the residual CFO degrades the channel estimate, and subsequently a poor estimate of the channel lead to a less accurate estimate of the residual CFO. These estimates can be improved by taking the following steps. We begin with an initial estimate of the channel. This estimate is used to obtain an estimate of the residual CFO using (66). The CFO estimate is then removed from $\mathrm{y}_{\mathrm{NMF}}$ and a second estimate of the channel is obtained. This will be followed by obtaining any remaining CFO, and removing it before proceeding with the detection of the payload part of the packet. Numerical results presented in the next section show that this single additional iteration significantly improves the estimated channel and CFO, hence, lead to a near optimum performance of the receiver.

F. MODIFIED NMF-BASED RECEIVER FOR HIGH SNR REGIME

As discussed in Section V, when compared to AFB-based receiver, the performance of the NMF-based receiver degrades at high levels of SNR. The observation made in Section V-B was that the NMF-based receiver can be made to perform similar to the AFB-based receiver if the signal power is removed from the power normalization coefficients. This, which may be seen as a deviation from the blind nature of the proposed receiver, can be done by taking the following steps.

After channel and CFO estimation, and removal of the residual CFO from the received signal, a period of the second part of the preamble (carrying multiple periods of the ZC sequence) is extracted. Then, the signal part of the extracted period is constructed and subtracted. Subsequently, the residual part, which contains only noise plus interference, is used to obtain the normalization coefficients q_k following the same procedure as the one outlined in Section III.

VII. SIMULATED RESULTS

In this section, we provide numerically simulated results to corroborate the findings of the previous sections. We begin by comparing the performance of the proposed NMF-based receiver against its AFB-based counterpart. With our target application in mind, we make this comparison through the presented uncoded BER curves under multipath channel models provided by the 3GPP. The efficacy of the MMSE channel estimator given by (46) is demonstrated through simulations under the expected usage scenarios. Next, the performance of the proposed fine CFO estimation method is explored by presenting couple of examples. We also assess the improvement to the CFO and channel estimates when the two methods are iterated.

A. UNCODED BER PERFORMANCE

In Section V, the AFB-based and NMF-based FBMC-SS symbol detectors were shown to be equivalent when the channel across each subcarrier band could be approximated by a flat gain and the transmission is made in a low SNR regime. To verify this result, here, we demonstrate the performance of both symbol detectors through MATLAB simulations. These simulations first produce a discrete-time FBMC-SS transmit signal according to (2) containing 1024 random BPSK data symbols and sampled at the Nyquist rate of $f_{\mathrm{Nyq}} = 2K/T_s$. The preamble symbols are also added. Following the implementations of [7], the symbol rate is set

to $1/T_s = 250$ kHz, and the prototype filter $h(t)$ is a square-root raised-cosine pulse-shape with roll-off factor $\alpha = 1$, truncated to a period of $N = 6$ symbols. The generated transmit signal is then passed through a multipath channel $c(t)$ following (14), and AWGN with the two-sided noise power spectral density $N_o/2$ is added to this signal. Taking note that the signal of interest has a bandwidth of $2K/T_s$ (spanned over the range $-K/T_s < f < K/Ts$), and is sampled at the Nyquist rate $f_{\text{Nyq}} = 2K/T_s$, one finds that the added noise has the power/variance of $\sigma_v^2 = \frac{K}{T_s} N_o$. Accordingly, the SNR is defined as the ratio of the received signal power (denoted by σ_r^2) over the noise power σ_v^2, viz.,

$$\text{SNR} = \frac{\sigma_r^2}{\sigma_v^2}. \tag{68}$$

Furthermore, taking note that each BPSK symbol carries a single bit, one finds that, here, the energy per bit can be expressed as $E_b = \sigma_r^2 T_s$. This leads to the following relationship between SNR and E_b/N_o:

$$E_b/N_o = K \cdot \text{SNR}. \tag{69}$$

It should be further noted that, here, E_b/N_o is defined at the receiver input, prior to any matched filtering.

Additional Gaussian noise with a flat power spectral density over each subcarrier band is added to serve as an interfering signal over a range of the selected subcarriers. The distorted signal is finally passed to the receiver where symbol estimates are obtained for the respective receivers.

It is assumed that the channel response is known to the receivers, and the channel is static over the period of a packet. The particular channel models used in these results are the tapped delay line (TDL) models recommended for 5G system development by the 3GPP, [39]. The AFB-based receiver is provided the noise plus interference powers for each subcarrier, $\sigma_{v',k}^2$, such that optimal MRC can be performed. The NMF-based receiver, on the other hand, is given no such information, hence, the normalization coefficients are simply calculated using the measured signal power at the input to the receiver according to (11). With payload symbol detection being the primary focus of these designs, the results here are presented in terms of uncoded bit-error rate (BER). The results are averaged over 1000 independent channel and noise/interference realizations.

Figure 9 presents the simulated BER curves under a TDL-A channel model with a "short" RMS delay spread of 30 ns, [39]. Two cases of $K = 64$ and $K = 256$ subcarriers are explored following the previous studies in [6] and [7]. An interfering signal at 30 dB above the signal level is applied over 1/4 of the subcarriers, namely, $k \in [0, 15]$ and $k \in [0, 63]$ for $K = 64$ and $K = 256$, respectively. These results clearly confirm similar performance of NMF-based and AFB-based receivers, in the present case. Also presented in Fig. 9 are BER curves for an SMF-based detector in the presence of interference. This detector is implemented as in Fig. 3.

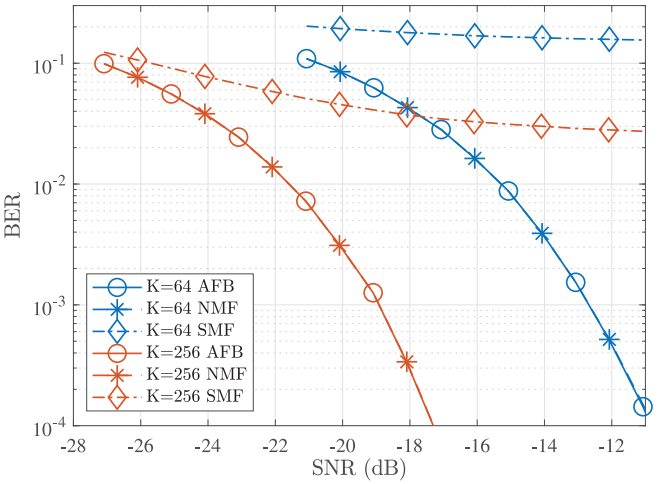

FIGURE 9. Simulated BERs for SMF-, NMF-, and AFB-based receivers. The channel model is TDL-A with 30 ns RMS delay spread, and symbol rate is at $1/T_s = 250$ kHz. Interfering signal is at 30 dB above signal level and covers 25% of the transmission band.

Simulated results under harsher channel conditions are presented in Fig. 10. Here, the channel model follows the TDL-C power-delay profile with a "very-long" delay spread of 1 μs, [39], while all other parameters match the previous test case. Here, some small improvement of the NMF-based receiver over its AFB counterpart is observed. We attribute this improvement to the spread of the transmit energy over a set of multipaths whose span is comparable to T_s. The NMF-based receiver has the ability to collect the energy from the multipaths more effectively than the AFB-based receiver. A formal evaluation of the impact of multipaths energy distribution in the AFB-based receiver is provided in [13], wherein it is demonstrated that the effective channel response over each subcarrier band becomes attenuated as the channel delay spread increases. This is because the signals from various paths may not be combined efficiently at the output of AFB in this scenario. The NMF-based receiver, on the other hand, separates the multipaths and applies a RAKE combining to them using the matched filter $c^*(-t)$ as demonstrated in Fig. 4.

To test the above hypothesis further, the symbol rate is quadrupled to the value of $1/T_s = 1$ MHz and the results are presented Fig. 11. Here, we observe that while the performance of the NMF-based receiver has remained about the same when compared to the results in Fig. 10, the AFB-based receiver shows a loss of 3 to 4 dB. This loss may be recovered to some extent by using a RAKE receiver in the manner discussed in [13], which clearly adds more complexity to the receiver.

B. CHANNEL ESTIMATOR

Here, we provide simulated results to demonstrate the performance of the MMSE channel estimator outlined in Section VI-B. As mentioned there, the channel covariance matrix $\mathbf{\Sigma_{cc}}$ may not have a true inverse when the number of channel paths N_{c_i} is less than L_c. The alternate form of

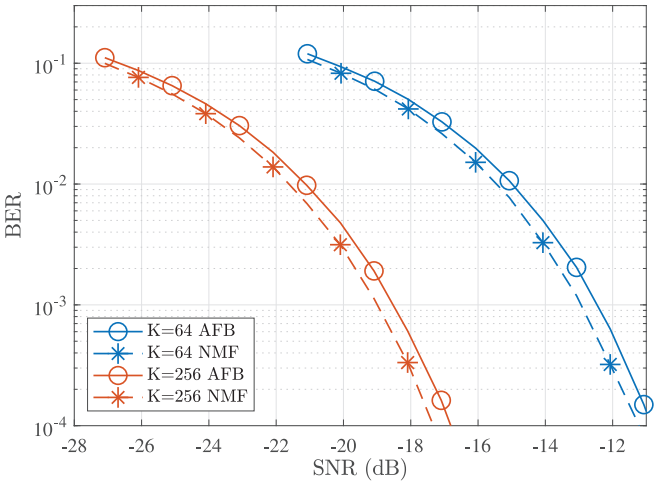

FIGURE 10. Simulated BERs of NMF-based and AFB-based receivers. The channel model is TDL-C with 1 μs RMS delay spread, and symbol rate is at $1/T_S = 250$ kHz. Interfering signal is at 30 dB above signal level and covers 25% of the transmission band.

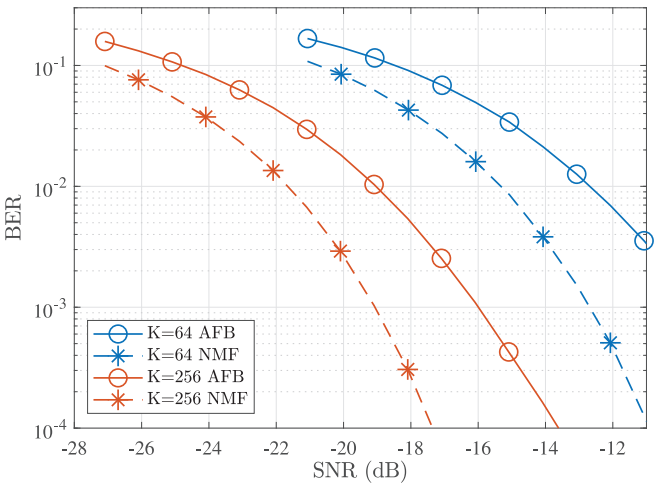

FIGURE 11. Simulated BERs of NMF-based and AFB-based receivers. The channel model is TDL-C with 1 μs RMS delay spread, and symbol rate is at $1/T_S = 1$ MHz. Interfering signal is at 30 dB above signal level and covers 25% of the transmission band.

the MMSE estimator given by [38, eq. (10.28)] may be used in this case, as it requires no inverse of $\mathbf{\Sigma_{cc}}$. However, to keep the complexity low, the formulation of (46) is preferred. When $L_c > N_{c_i}$, a small positive regularization constant may be added to the diagonal elements of $\mathbf{\Sigma_{cc}}$. For the results presented here, we let this regularization constant to be

$$\lambda = 10^{-6} \times \text{mean}(\text{diag}(\mathbf{\Sigma_{cc}})). \tag{70}$$

To characterize the loss induced due to the added regularization constant, the estimators (46) and [38, eq. (10.28)] are compared. Note that the estimator form used here follows (46) and not (48), that is, the receiver is provided the exact $\mathbf{\Sigma}_{\mathbf{v}'_\mathrm{f}\mathbf{v}'_\mathrm{f}}$. These simulations first generate the NMF output for a transmitted preamble according to (41). There are $K = 64$ subcarriers with a symbol rate of 250 kHz, and the ZC sequence contains $Z = 16$ symbols. A partial-band

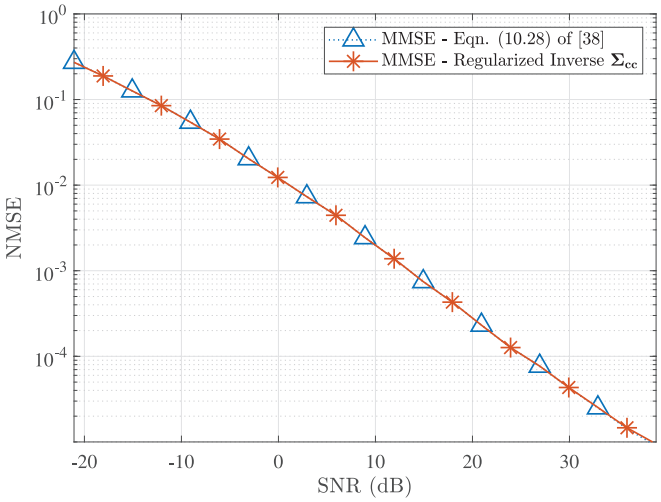

FIGURE 12. Ideal vs. sub-optimal MMSE channel estimator performance with $K = 64$ subcarriers, TDL-A channel with 30ns RMS delay spread. Interfering signal is at 30 dB above signal level over 25% of subcarrier bands.

interfering signal with a power 30 dB above the signal level is applied to subcarriers $k \in [0, 15]$. The channel follows the TDL-A profile containing $N_{c_i} = 23$ discrete paths, with an RMS delay spread of 30 ns, [39]. A total of 1000 independent channel realizations are simulated. The length of the channel estimate is $L_c = 25$. The channel power is normalized to $\mathbf{c}^{\mathrm{H}}\mathbf{c} = 1$. Figure 12 presents the normalized mean-squared error (NMSE) of the resulting channel estimates. The result here demonstrates that the addition the regularization constant λ has no noticeable impact on the estimated channel over the full range of SNR values simulated.

We next examine the performance loss when $\mathbf{\Sigma}_{\mathbf{v}'_\mathrm{f}\mathbf{v}'_\mathrm{f}}$ is estimated. In the NMF-based receiver, such estimate is obtained by estimating the received signal power (including, noise and interference) over each subcarrier band. We also recall that the simplified form (48) assumes that the receiver operates in a low SNR regime (negative SINR), hence, the approximation (47) holds. Since the normalization coefficients become more affected by the signal power as SNR increases, this approximation is violated, resulting in a sub-optimal estimator. Using the same parameters as before, the performance of estimators (46) and (48) are simulated, and the results are visualized in Fig. 13. Here, we see that the performance of (46) and (48) matches at low SNR as expected, but the latter exhibits some loss in high SNR range. Figure 13 also presents the theoretical error bound of (51). The estimator (46) follows this bound, as one would expect.

For completeness of our results here, and in order to emphasize the significance of adopting the MMSE channel estimator (46), we also examine the performance of the popular minimum-variance unbiased (MVU) channel estimator. The MVU estimator follows the same form as (48), with the term $\mathbf{\Sigma}_{\mathbf{cc}}^{-1}$ removed; see [38, Th. 4.1] for details. The performance of this estimator is also given in Fig. 13. Here, we observe a significant loss in performance which may

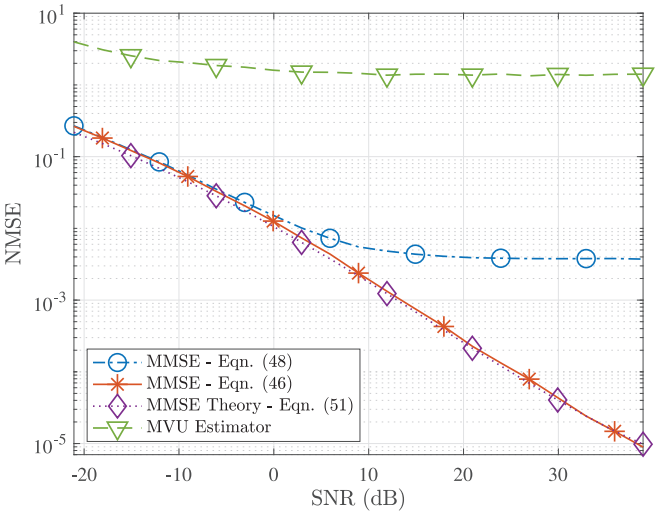

FIGURE 13. Channel estimator performance with $K = 64$ subcarriers, TDL-A channel with 30 ns RMS delay spread. Interfering signal is at 30 dB above signal level over 25% of subcarrier bands.

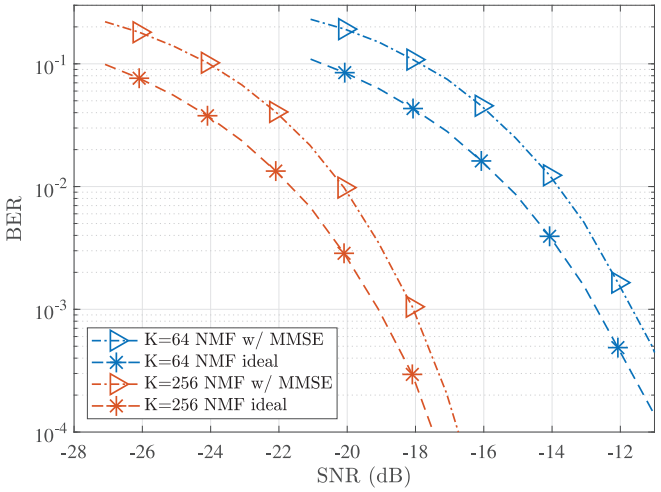

FIGURE 14. Simulated BERs of the NMF-based receiver with known and estimated channel response. The channel model is TDL-C with 1 μs RMS delay spread, and symbol rate is at $1/T_S = 1$ MHz. Interfering signal is at 30 dB above signal level and covers 25% of the transmission band.

be explained as follows. The MVU estimator is known to incur some noise/interference enhancement, especially when the noise/interference is highly colored. This is because the MVU estimator, by definition, provides an *unbiased* estimate of the desired underlying parameters, no matter how large the variance of the estimates (caused by noise/interference) will be. Hence, the MVU estimator may exhibit poor performance with high levels of noise/interference. It should be further noted that in the example given in Fig. 13, the interfering signal over 25% of the subcarrier bands is the main source of the degradation. Because the level of the interfering signal here is 30 dB above the signal level regardless of the SNR value, the error of the MVU estimator remains high across the full range of SNRs given in Fig. 13. The MMSE estimator, on the other hand, strikes a balance between any bias in the estimated channel and minimization of the estimation error cause by noise/interference. When the received signal is free of high-power partial band interference, we have found that the simulated performance of the MVU estimator greatly improves, but still lags the performance of the MMSE estimator. Considering the target use cases of FBMC-SS, we have omitted the results for such a scenario here for brevity.

Another point that is worth noting here is that a satisfactory implementation of the MMSE estimator does not require an accurate estimate of $\mathbf{\Sigma_{cc}}$. A coarse estimate of $\mathbf{\Sigma_{cc}}$ can be easily obtained by taking the following steps: (i) By making use of the autocorrelation property of the ZC sequences, a coarse estimate of the channel impulse response $\mathbf{c}$ can be obtained by circularly convolving $\mathrm{y_{NMF}}$ with the expanded, time-reversed, and conjugated version of $\mathrm{s_{ZC}}$. (ii) The squared magnitude of the estimated channel elements are then used to form the diagonal elements of the diagonal matrix $\mathbf{\Sigma_{cc}}$. Moreover, as noted earlier, a small regularization factor is add to the diagonal elements of $\mathbf{\Sigma_{cc}}$ to resolve any ill-conditioning.

Finally, to complete our discussion here, we examine the impact of the estimated channel on the BER results. We have run simulations for all three cases that are presented in Figs. 9, 10, and 11, and the BER results when the channel was estimated were compared against the results where the channel was known perfectly. The observation was that the performance loss caused by the channel estimate (the MMSE estimator) was in the order of 1 dB or less. A sample example of this study is presented in Fig. 14.

C. CFO ESTIMATOR

We will now shift our focus to the residual CFO estimator presented in Section VI-D. The same parameters as those in Section VII-B are used, and the results are averaged over an ensemble of 1000 realizations. For the results provided here, we set the E_b/N_o to a level of 6 dB, corresponding to an SNR $= 6 - 10\log_{10} 64 \approx -12$ dB. First, we examine the means of the CFO estimate (66) for different overlap factors M. The normalized mean absolute error of CFO estimates, defined as $T_s \times \mathrm{mean}(|\delta_f - \hat{\delta}_f|)$, is visualized in Fig. 15.

The results presented in Fig. 15 indicate that higher values of M will result in a lower expected error. However, at the higher range of CFO values, the mean error for $M = 16$ case increases rapidly compared to the other curves. This may be explained as follows. For $M = 16$, as $\delta_f T_s Z$ approaches 0.5, $\angle(\hat{\mathbf{c}}_{a,0}^{\mathrm{H}} \hat{\mathbf{c}}_{b,0})$ approaches the ambiguous bounds $\pm\pi$, hence, the noise may occasionally push the measured phase past these bounds, leading to catastrophically large errors. Considering this observation, it may be reasonable to choose M slightly less than Z. The choice of $M = 12$ is a good compromised value.

Next, the process of iterating the proposed channel and CFO estimation methods as described in Section VI-E is simulated. We set $M = 12$ and $E_b/N_o = 6$ dB. Table 1 presents results for the mean absolute values of CFO error, normalized

TABLE 1. Normalized mean absolute error of CFO estimates upon iterating CFO and channel estimation methods.

		Iteration			
		0	1	2	3
Rel. CFO $\delta_f T_s Z$	0	1.72×10^{-3}	1.72×10^{-3}	1.73×10^{-3}	1.73×10^{-3}
	0.1	1.78×10^{-3}	1.75×10^{-3}	1.76×10^{-3}	1.76×10^{-3}
	0.2	1.89×10^{-3}	1.76×10^{-3}	1.77×10^{-3}	1.77×10^{-3}
	0.3	2.00×10^{-3}	1.79×10^{-3}	1.80×10^{-3}	1.80×10^{-3}
	0.4	2.30×10^{-3}	1.87×10^{-3}	1.88×10^{-3}	1.88×10^{-3}
	0.5	2.84×10^{-3}	2.04×10^{-3}	2.03×10^{-3}	2.03×10^{-3}

Normalized mean error magnitude $|\delta_f - \hat{\delta}_f| \times T_s$

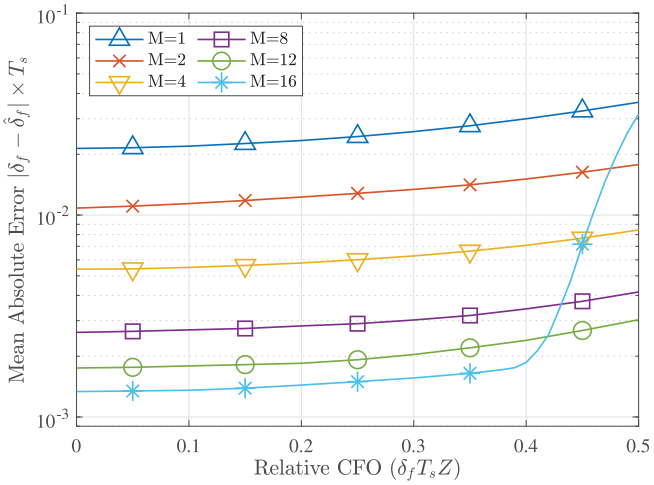

FIGURE 15. CFO estimator performance with $K = 64$ subcarriers, TDL-A channel with 30 ns RMS delay spread. Interfering signal at 30dB above signal level over 25% of subcarrier bands.

TABLE 2. Normalized MSE of channel estimates upon iterating CFO and channel estimation methods.

		Iteration			
		0	1	2	3
Rel. CFO $\delta_f T_s Z$	0	0.134	0.156	0.157	0.157
	0.1	0.217	0.158	0.158	0.158
	0.2	0.446	0.162	0.161	0.161
	0.3	0.764	0.167	0.165	0.165
	0.4	1.094	0.173	0.170	0.170
	0.5	1.360	0.182	0.174	0.174

NMSE of channel estimate $\hat{\mathbf{c}}$

to the symbol rate $1/Ts$, over 3 iterations. The corresponding MSE of channel estimates, normalized to channel norm $\mathbf{c}^H\mathbf{c}$, are presented in Table 2. From the tables, we note that there is a noticeable improvement to the channel and CFO estimates upon the first iteration. However, there is little to no improvement over subsequent iterations. Hence, we may conclude one iteration is sufficient.

At this point, we provide an example to make some comments that relate the lock ranges of the coarse and fine CFO estimators to the required accuracy of a free running oscillator at the receiver. For the parameters used in this section, the lock range (61), with $\psi = 0.5$, reduces to the range $|\delta_f| < 250/32 = 7.8$ kHz. Assuming a carrier frequency 2.4 GHz, this lock range would be satisfied, i.e., no coarse CFO estimation would be required, if the receiver local oscillator had an accuracy of better than $\frac{7.8\times10^3}{2.4\times10^9} \equiv 3.25$ ppm, where 'ppm' stands for part per million. This is a relatively tight requirement as common oscillators usually have an accuracy of 10 or 20 ppm. Hence, as discussed in the previous sections, a coarse CFO estimation may be necessary.

A possible method of extending the lock range and, thus, be able to obtain a coarse estimate of CFO such that the residual CFO falls within the above range, is to adopt the method proposed in [7]. In this work, the authors suggest that the packet preamble starts with a long sequence of ± 1 that are used for both packet detection and CFO estimation. Since this sequence has a period of $2T_s$, when used for CFO estimation, it provides a lock range of $-\frac{1}{4Ts} < \Delta_f < \frac{1}{4T_s}$, which for the choice of $1/Ts = 250$ kHz, corresponds to the range $|\Delta_f| < 62.5$ kHz. For the case considered above, this can support local oscillators with an accuracy of as large as $\frac{62.5\times10^3}{2.4\times10^9} \equiv 26$ ppm.

VIII. COMPARISONS

Comparing alternative algorithms that perform similar tasks is traditionally done by counting the number of multiply/add operations that they require to complete the task. Such comparison may not be meaningful in modern implementations, where receivers are often implemented in application-specific integrated circuits (ASIC) or programmed into field-programmable gate array (FPGA) chips. In such implementations, majority of savings comes from reusing similar blocks for different tasks. The complexity comparison that is presented here takes this point of view.

The FBMC-SS receiver, the subject of this paper, needs to complete the following tasks to detect an incoming data packet and recover its information content.

1) Detect the arrival of the packet at the receiver input.
2) Perform carrier and timing synchronization tasks.
3) Obtain the channel state information (CSI) including the noise plus interference level for each subcarrier band.
4) Set the receiver parameters for data detection and proceed with information recovery.

In the context of this paper, both receiver structures (AFB-based and NMF-based) make use of the NMF and other similar signal processing steps to complete Tasks 1), 2), and

3). The difference appears only in Task 4) where the NMF-based receiver may continue to use the already constructed NMF block for data detection. The AFB-based receiver, on the other hand, has to construct and utilize a new signal processing block, namely, an analysis filter bank, for data detection. Accordingly, we argue that the NMF-based receiver is less complex to implement than its AFB-based counterpart.

In terms of performance, the observation made in the previous section suggests that while the two receivers perform similarly for many typical use cases, under certain channel conditions, the NMF-based receiver may outperform the AFB-based receiver. This is the case when the channel impulse response spans over a large fraction of the symbol interval. The high resolution of the NMF in separating the multi-paths of the channel allows for trivial combining of the signal energy in these paths, leading to improved performance of the receiver. Such resolution is non-existent in the AFB-based receiver.

IX. CONCLUSION

In this work, we presented an extension to an existing FBMC-SS packet detector to enable robust symbol detection with blind interference suppression. Through a slight modification of the normalization coefficients and cascading with a RAKE detector, the NMF-based receiver may achieve a similar or better performance than the well-established AFB-based designs of [6], [7], and [40]. Analysis demonstrating the equivalence of the two receiver designs in channels with frequency-flat fading over each subcarrier at low SNR was presented. Details of a candidate receiver design utilizing this detector were presented, with specific methods given for the channel and CFO estimation components. The performance loss of the channel estimator due to a residual CFO was considered, and simulated results were provided to validate the findings. A modification allowing the receiver to perform optimally over the full range of SNRs was also outlined. Finally, simulated results were presented to confirm the given analyses and to demonstrate the efficacy of the proposed receiver design.

REFERENCES

[1] R. Pickholtz, D. Schilling, and L. Milstein, "Theory of spread-spectrum communications—A tutorial," *IEEE Trans. Commun.*, vol. TC-30, no. 5, pp. 855–884, May 1982.

[2] S. Hara and R. Prasad, "Overview of multicarrier CDMA," *IEEE Commun. Mag.*, vol. 35, no. 12, pp. 126–133, Dec. 1997.

[3] S. Kondo and L. B. Milstein, "Performance of multicarrier DS CDMA systems," *IEEE Trans. Commun.*, vol. 44, no. 2, pp. 238–246, Feb. 1996.

[4] G. K. Kaleh, "Performance comparison of frequency-diversity and frequency-hopping spread-spectrum systems," *IEEE Trans. Commun.*, vol. 45, no. 8, pp. 910–912, Aug. 1997.

[5] B. Farhang-Boroujeny and C. Furse, "A robust detector for multicarrier spread spectrum transmission over partially jammed channels," *IEEE Trans. Signal Process.*, vol. 53, no. 3, pp. 1038–1044, Mar. 2005.

[6] D. L. Wasden, H. Moradi, and B. Farhang-Boroujeny, "Design and implementation of an underlay control channel for cognitive radios," *IEEE J. Sel. Areas Commun.*, vol. 30, no. 10, pp. 1875–1889, Nov. 2012.

[7] T. Haddadin *et al.*, "An underlay communication channel for 5G cognitive mesh networks: Packet design, implementation, analysis, and experimental results," in *Proc. IEEE Int. Conf. Commun. Workshops (ICC)*, Kuala Lumpur, Malaysia, May 2016, pp. 498–504.

[8] L. Lampe and K. Witrisal, "Challenges and recent advances in IR-UWB system design," in *Proc. IEEE Int. Symp. Circuits Syst.*, Paris, France, May 2010, pp. 3288–3291.

[9] Q. Zhou, Z. Zou, Q. Chen, H. Tenhunen, and L.-R. Zheng, "Low complexity burst packet detection for wireless-powered UWB RFID systems," in *Proc. IEEE Int. Conf. Ubiquitous Wireless Broadband (ICUWB)*, Montreal, QC, Canada, Oct. 2015, pp. 1–5.

[10] B. Miscopein and J. Schwoerer, "Low complexity synchronization algorithm for non-coherent UWB-IR receivers," in *Proc. IEEE 65th Veh. Technol. Conf. (VTC-Spring)*, Dublin, Ireland, Apr. 2007, pp. 2344–2348.

[11] D. Dardari, C.-C. Chong, and M. Win, "Threshold-based time-of-arrival estimators in UWB dense multipath channels," *IEEE Trans. Commun.*, vol. 56, no. 8, pp. 1366–1378, Aug. 2008.

[12] T. Sibbett, H. Moradi, and B. Farhang-Boroujeny, "Normalized matched filter for blind interference suppression," in *Proc. IEEE Mil. Commun. Conf. (MILCOM)*, Los Angeles, CA, USA, Oct. 2018, pp. 1–6.

[13] S. A. Laraway and B. Farhang-Boroujeny, "Performance analysis of a multicarrier spread spectrum system in doubly dispersive channels with emphasis on HF communications," *IEEE Open J. Commun. Soc.*, vol. 1, pp. 462–476, 2020.

[14] D. B. Haab, H. Moradi, and B. Farhang-Boroujeny, "Filter bank multi-carrier spread spectrum with biorthogonal signaling for high speed data transmission through HF skywave channels," in *Proc. IEEE Mil. Commun. Conf. (MILCOM)*, Los Angeles, CA, USA, Oct. 2018, pp. 1–9.

[15] G. Forney, "Maximum-likelihood sequence estimation of digital sequences in the presence of intersymbol interference," *IEEE Trans. Inf. Theory*, vol. IT-18, no. 3, pp. 363–378, May 1972.

[16] A. M. Monk, M. Davis, L. B. Milstein, and C. W. Helstrom, "A noise-whitening approach to multiple access noise rejection .I. Theory and background," *IEEE J. Sel. Areas Commun.*, vol. 12, no. 5, pp. 817–827, Jun. 1994.

[17] L. Wei and L. K. Rasmussen, "A near ideal noise whitening filter for an asynchronous time-varying CDMA system," *IEEE Trans. Commun.*, vol. 44, no. 10, pp. 1355–1361, Oct. 1996.

[18] T. Kailath, "An innovations approach to least-squares estimation–part I: Linear filtering in additive white noise," *IEEE Trans. Autom. Control*, vol. AC-13, no. 6, pp. 646–655, Dec. 1968.

[19] J. Xie, Y. Yuan, and Y. Liu, "Super-resolution processing for HF surface wave radar based on pre-whitened MUSIC," *IEEE J. Ocean. Eng.*, vol. 23, no. 4, pp. 313–321, Oct. 1998.

[20] D. G. Childers, D. P. Skinner, and R. C. Kemerait, "The cepstrum: A guide to processing," *Proc. IEEE*, vol. 65, no. 10, pp. 1428–1443, Oct. 1977.

[21] J. P. Le Cadre, "Parametric methods for spatial signal processing in the presence of unknown colored noise fields," *IEEE Trans. Acoust., Speech, Signal Process.*, vol. 37, no. 7, pp. 965–983, Jul. 1989.

[22] F. Hsu and A. Giordano, "Digital whitening techniques for improving spread spectrum communications performance in the presence of narrowband jamming and interference," *IEEE Trans. Commun.*, vol. 26, no. TC-2, pp. 209–216, Feb. 1978.

[23] J.-Z. Fu, L.-L. Guo, H.-Q. Yang, and Z.-X. Han, "Narrow-band interference suppression in DSSS systems using efficient adaptive filters," in *Proc. WRI Int. Conf. Commun. Mobile Comput.*, vol. 1. Kunming, China, 2009, pp. 353–357.

[24] J. Wang, "Adaptive filter for suppressing narrow-band interference in DSSS communication," in *Proc. Int. Conf. Comput. Sci. Serv. Syst. (CSSS)*, Nanjing, China, 2011, pp. 162–165.

[25] L. Ping and R. Lu, "An improved variable step-size affine projection algorithm for narrowband interference suppression in DSSS systems," in *Proc. Int. Conf. Qual. Rel. Risk Maint. Safety Eng. (QR2MSE)*, Chengdu, China, 2013, pp. 2043–2046.

[26] D. Zhao, B. Jia, J. Ding, and W. Cui, "Narrow-band interference suppression in DSSS using dual-threshold algorithm," in *Proc. IET Int. Radar Conf.*, Hangzhou, China, 2015, pp. 1–5.

[27] X. Tan, S. Su, and X. Sun, "Research on narrowband interference suppression technology of UAV network based on spread spectrum communication," in *Proc. IEEE Int. Conf. Artif. Intell. Inf. Syst. (ICAIIS)*, Dalian, China, 2020, pp. 335–338.
[28] B. Shen and X. Shi, "A novel frequency domain narrowband interference suppression algorithm based on noncoherent accumulation," in *Proc. IEEE 3rd Int. Conf. Comput. Commun. Eng. Technol. (CCET)*, Beijing, China, 2020, pp. 308–313.
[29] Y. Jiang, H.-Y. Gao, and S.-P. Yu, "Adaptive interference excision in digital spread spectrum communication systems based on wavelet packet transform," in *Proc. Int. Conf. Mach. Learn. Cybern.*, vol. 6. Hong Kong, 2007, pp. 3278–3282.
[30] J. J. Perez-Solano, S. Felici-Castell, and M. A. Rodriguez-Hernandez, "Narrowband interference suppression in frequency-hopping spread spectrum using undecimated wavelet packet transform," *IEEE Trans. Veh. Technol.*, vol. 57, no. 3, pp. 1620–1629, May 2008.
[31] B. Farhang-Boroujeny, *Signal Processing Techniques for Software Radios*, 2nd ed., Morrisville, NC, USA: Lulu Publ. House, 2010.
[32] P. Vaidyanathan, *Multirate Systems and Filter Banks*. Englewood Cliffs, NJ, USA: Prentice-Hall, 1993.
[33] R. Frank, S. Zadoff, and R. Heimiller, "Phase shift pulse codes with good periodic correlation properties (corresp.)," *IRE Trans. Inf. Theory*, vol. 8, no. 6, pp. 381–382, Oct. 1962.
[34] D. Chu, "Polyphase codes with good periodic correlation properties (corresp.)," *IEEE Trans. Inf. Theory*, vol. IT-18, no. 4, pp. 531–532, Jul. 1972.
[35] Y. T. Li and R. Wong, "Integral and series representations of the dirac delta function," *Commun. Pure Appl. Anal.*, vol. 7, no. 2, pp. 229–247, 2008.
[36] J. H. J. Iinatti, "On the threshold setting principles in code acquisition of DS-SS signals," *IEEE J. Sel. Areas Commun.*, vol. 18, no. 1, pp. 62–72, Jan. 2000.
[37] R. Gray, *Toeplitz and Circulant Matrices: A Review* (Foundations and Trends in Technology). Boston, MA, USA: Now Publ., 2006.
[38] S. M. Kay, *Fundamentals of Statistical Signal Processing: Estimation Theory*, vol. 1. Englewood Cliffs, NJ, USA: Prentice-Hall, 1993.
[39] "Study on channel model for frequencies from 0.5 to 100 GHz," 3rd Gener. Partnership Project, Sophia-Antipolis, France, 3GPP Rep. TR 38 901, 2019.
[40] S. A. Laraway, H. Moradi, and B. Farhang-Boroujeny, "HF band filter bank multi-carrier spread spectrum," in *Proc. IEEE Mil. Commun. Conf.*, Tampa, FL, USA, Oct. 2015, pp. 1445–1453.

DAVID B. HAAB received the B.S. and M.S. degrees in electrical engineering from the University of Utah in 2019. He is currently pursing the Ph.D. degree in electrical engineering under the supervision of Dr. B. Farhang-Boroujeny. He is currently a Research Assistant with the Wireless Communications Lab, University of Utah, working in conjunction with Idaho National Laboratory to develop next-generation radio systems. His research interests include cognitive radio, multicarrier communications, spread-spectrum waveforms, and software-defined radio implementation.

HUSSEIN MORADI (Member, IEEE) received the bachelor's degree from the University of Texas at Arlington, Arlington, TX, USA, and the master's and Ph.D. degrees from Southern Methodist University, Dallas, TX, USA.

He held director positions for wireless research and development with Kyocera Wireless, VeriFone Inc., and NEC America, advancing state-of-the-art wireless devices. In 2009, he joined the Idaho National Laboratory as a Chief Wireless Scientist for National and Homeland Security. He brings over 30 years of experience incorporate research and leadership development. He has developed GSM/GPRS/EDGE, CDMA/EVDO, 802.11, BT 2.5G/3G VoIP wireless handsets and has domain expertise in WiMAX, LTE, and physical-layer spectrum agile communication technologies. As a recognized national thought leader in telecommunications, he holds five international patents in spectrum sharing and three pending in wireless communications systems shaping the next generation wireless global standardization. His research interests include systems engineering, RF layer, ASIC, hardware and embedded software development for computing and wireless telecommunications devices. He received the 2012 Research and Development 100 Award for his wireless spectrum communication system innovation.

BEHROUZ FARHANG-BOROUJENY (Life Senior Member, IEEE) received the B.Sc. degree in electrical engineering from Teheran University, Iran, in 1976, the M.Eng. degree from the University of Wales Institute of Science and Technology, U.K., in 1977, and the Ph.D. degree from Imperial College, University of London, U.K., in 1981.

From 1981 to 1989, he was with the Isfahan University of Technology, Isfahan, Iran. From 1989 to 2000, he was with the National University of Singapore. Since August 2000, he has been with the University of Utah. He is an Expert in the general area of signal processing. He has worked and has made significant contribution to areas of adaptive filters theory, acoustic echo cancelation, magnetic/optical recoding, and digital subscriber line technologies. He has authored the books *Adaptive Filters: Theory and Applications* (Wiley, 1998 (1st ed.) and 2013 (2nd ed.)] and *Signal Processing Techniques for Software Radios* [LuluPublishing House, 2009 (1st ed.) and 2010 (2d ed.)]. His current scientific interests are adaptive filters, multicarrier communications, detection techniques for space–time coded systems, and cognitive radio. He served as an Associate Editor for the IEEE TRANSACTIONS ON SIGNAL PROCESSING from July 2002 to July 2005, and IEEE SIGNAL PROCESSING LETTERS from April 2008 to March 2010. He has also been involved in various IEEE activities, including the Chairmanship of the Signal Processing/Communications Chapter of IEEE, Utah, from 2004 to 2005.